Variations of Sea Surface Temperature, Wind Stress, and Rainfall over the Tropical Atlantic and South America

PAULO NOBRE AND J. SHUKLA

Center for Ocean–Land–Atmosphere Studies, Institute for Global Environment and Society, Calverton, Maryland

(Manuscript received 21 March 1994, in final form 12 March 1996)

ABSTRACT

Empirical orthogonal functions (EOFs) and composite analyses are used to investigate the development of sea surface temperature (SST) anomaly patterns over the tropical Atlantic. The evolution of large-scale rainfall anomaly patterns over the equatorial Atlantic and South America are also investigated. The EOF analyses revealed that a pattern of anomalous SST and wind stress asymmetric relative to the equator is the dominant mode of interannual and longer variability over the tropical Atlantic. The most important findings of this study are as follows.

Atmospheric circulation anomalies precede the development of basinwide anomalous SST patterns over the tropical Atlantic. Anomalous SST originate off the African coast simultaneously with atmospheric circulation anomalies and expand westward afterward. The time lag between wind stress relaxation (strengthening) and maximum SST warming (cooling) is about two months.

Anomalous atmospheric circulation patterns over northern tropical Atlantic are phase locked to the seasonal cycle. Composite fields of SLP and wind stress over northern tropical Atlantic can be distinguished from random only within a few months preceding the March–May (MAM) season. Observational evidence is presented to show that the El Niño–Southern Oscillation phenomenon in the Pacific influences atmospheric circulation and SST anomalies over northern tropical Atlantic through atmospheric teleconnection patterns into higher latitudes of the Northern Hemisphere.

The well-known droughts over northeastern Brazil (Nordeste) are a local manifestation of a much larger-scale rainfall anomaly pattern encompassing the whole equatorial Atlantic and Amazon region. Negative rainfall anomalies to the south of the equator during MAM, which is the rainy season for the Nordeste region, are related to an *early* withdrawal of the intertropical convergence zone toward the warm SST anomalies over the northern tropical Atlantic. Also, it is shown that precipitation anomalies over southern and northern parts of the Nordeste are out of phase: drought years over the northern Nordeste are commonly preceded by wetter years over the southern Nordeste, and vice versa.

1. Introduction

One of today's most challenging problems for long-range forecasting of tropical rainfall is an accurate prediction of sea surface temperature (SST) over the Tropics. There is a large body of evidence in the literature that suggests time-mean area-averaged rainfall over the Tropics is modulated by slowly varying boundary conditions like SST and soil moisture (Shukla 1984; Dirmeyer and Shukla 1993). The interannual variability of SSTs over the tropical Atlantic, though smaller than the amplitude of its annual cycle (Merle and Hisard 1980; Hastenrath 1984), has a strong influence on the distribution of rainfall over the tropical Americas (Hastenrath and Heller 1977; Moura and Shukla 1981; Hastenrath 1984; Nobre and Shukla 1991) and Africa (Lamb 1978a,b; Lough 1986; Palmer 1986; Parker et al. 1988). For instance, anomalous meridional gradient of SST over the equatorial Atlantic has a profound impact on the total rainfall over northeastern Brazil (Nordeste) through the modulation of the intertropical convergence zone (ITCZ) latitudinal positioning (Hastenrath 1984; Hastenrath and Greischar 1993). The pattern of anomalous SSTs over the tropical Atlantic that is most often associated with years of drought or flood over Nordeste shows anomalies of opposite signs to the north and south of the equator (Hastenrath and Heller 1977; Markham and McLain 1977; Moura and Shukla 1981; Servain 1991). The interhemispheric asymmetry of SST anomalies in the tropical Atlantic and its relation to regional rainfall departures has been earlier reported by Hastenrath and Heller (1977), Hastenrath (1978), Lamb (1978a,b), Hastenrath (1984), and Hastenrath and Druyan (1993).

If SST anomalies could be predicted over the Tropics, it would be possible to make substantial improvements in long-range prediction of rainfall anomalies over the Nordeste (Ward and Folland 1991). However,

Corresponding author address: Dr. Paulo Nobre, Centro de Previsao de Temp e Estudos Climáticos, Instituto Nacional de Pesquisas Espaciais, Rodovia Presidente Dutra, Km 40, Cachoeira Paulista, SP, Brazil.

the mechanisms responsible for the development of anomalous SST patterns over the tropical Atlantic are yet largely unknown. There is some evidence that interannual variability of SST over the tropical Atlantic is achieved through both local dynamics and remotely forced perturbations, as those associated with the El Niño–Southern Oscillation (ENSO) phenomenon (Hastenrath et al. 1987; Aceituno 1988; Hameed et al. 1993; Curtis and Hastenrath 1995). Observational evidence and results of numerical simulations corroborate that positive values of the Southern Oscillation index (SOI) (indicating the cold phase of ENSO) are associated with concurrent anomalously colder SST and higher SLP over the northern tropical Atlantic and warmer SST and lower SLP over the southern tropical Atlantic, and vice versa (Hastenrath and Heller 1977; Hastenrath 1978; Hastenrath et al. 1987; Aceituno 1988; Hameed et al. 1993; Hastenrath and Greischar 1993). Also, the largest simultaneous correlation between the SOI and SST over the tropical Atlantic occurs during MAM (Ropelewski and Halpert 1987). Additionally, there is evidence that an El Niño-like phenomenon also takes place over the equatorial Atlantic (Philander and Pacanowski 1986; Zebiak 1993; Carton and Huang 1994). However, the "Atlantic ENSO" mode seems to be insufficiently strong to determine the total SST variability by itself, even close to the equator; thus, the total SST variability is to be achieved by the combined effects of ENSO-like equatorial coupling, other dynamical modes, and external or remotely forced perturbations (Zebiak 1993).

The question to be pursued in this paper is whether or not the ocean–atmosphere coupling over the tropical Atlantic is consistent with observations, and if so, what mechanisms of coupling are suggested. There is observational evidence that on the monthly timescale the SLP forcing of SST over the tropical Atlantic is stronger than the effect of SST on the atmospheric circulation (Lough 1986). The results of this work confirm previous findings and suggest that basinwide SST anomaly patterns develop from the interplay between hemispheric-scale atmospheric circulation disturbances and SST anomalies over the tropical Atlantic.

2. Data

The data used in this study are as follows: Sea surface temperature (SST) and wind stress (τ) from 30°S to 30°N over the tropical Atlantic are COADS 2° × 2° grid for the period January 1950 through December 1987, as in Halpert and Ropelewski (1989) [the pseudo-wind stress (units of $m^2 s^{-2}$) was converted into wind stress (units of dyn cm^{-2}) by Huang (1992)], horizontal winds at six levels from 48°S to 48°N are derived from the NMC operational analysis (Arkin 1982; Parish and Kistler 1982) for the period June 1974 through December 1987; sea level pressure (SLP) are COADS 2° × 2° grid between 60°S and 60°N from January 1946 through December 1985 (Slutz et al. 1985); global 2.5° × 2.5° gridded outgoing longwave radiation (OLR) for the period June 1974 through November 1990 (March through December 1978 missing) are from the National Meteorological Center (NMC); raingauge data over South America (north of 16°S) are from Departamento Nacional de Águas e Energia Elétrica (DNAEE), Brazil, for the period 1849–1984; and OLR-based precipitation estimates over the tropical Atlantic between 20°S and 20°N for the period June 1974–December 1988 (March through December 1978 missing) are from Yoo and Carton (1988).

All data are monthly. Anomalies are calculated as departures from the long-term mean at each grid point. Raingauge precipitation data over South America are averaged within 1° × 1° latitude–longitude boxes, generating one value per month per box in which measurements are available. Figure 1 shows the areas referred in the text as (A) eastern Amazon, (B) northern Nordeste, and (C) southern Nordeste.

3. Empirical orthogonal functions analysis

EOF analysis is used to identify the dominant modes of wind stress and SST variability over the tropical Atlantic. The data for the EOF calculations is sampled every other point from the 2° × 2° grid to produce a 4° × 4° grid. Departures from long-term (1964–1987) monthly means of SST and wind stress are normalized by their local standard deviations (Kutzbach 1967).

We shall focus on the eigenmodes (EOFs) of SST and wind stress that explain the largest portion of the variance during the periods in which variance is maximum. The maximum time variances of wind stress and SST over the northern tropical Atlantic occur during December–January–February (DJF) and March–April–May (MAM) respectively (figures not shown). Thus, the eigenanalysis is presented with data samples covering DJF-only, MAM-only, and 12-month data.

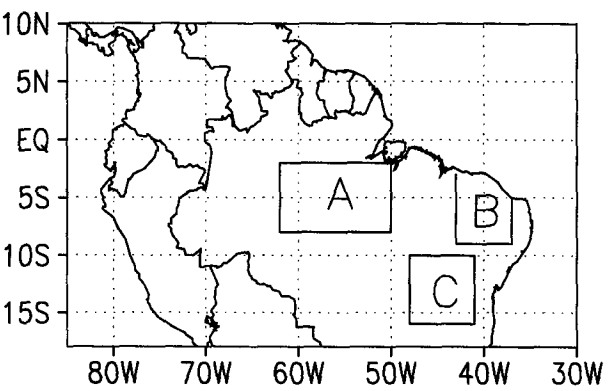

FIG. 1. Localization map. The (A) eastern Amazon, (B) northern Nordeste, and (C) southern Nordeste areas of Brazil are indicated.

The EOFs are calculated for each variable separately (SST, τ^X, τ^Y), jointly in pairs, and all three together.

The results of our calculations are discussed below, but only the first joint eigenvector of anomalous SST, τ^X, and τ^Y (hereafter called SST–τ–EOF1), for the 12-month data, and the first EOF of MAM-only anomalous SST are shown in Fig. 2 and Fig. 3, respectively. SST–τ–EOF1 (Fig. 2a) explains 13.1% of the total variance after subtracting the seasonal cycle. It shows that anomalous SST with opposite sign to the north and south of the equator are associated with anomalous τ^X with a similar dipole pattern and anomalous τ^Y directed from anomalously cold toward anomalously warm SST regions. Therefore, it suggests that warmer off-equatorial SSTs are associated with weaker trade winds and colder SSTs with stronger trade winds. SST–τ–EOF1 is of special importance to describe the interannual variability of the tropical Atlantic coupled ocean–atmosphere system since it brings together information on both SST and wind stress. The time series of coefficients associated with SST–τ–EOF1 (Fig. 2b) depicts a clear low-frequency decadal timescale, as well as superimposed interannual variability. The study of fluctuations of decadal or longer timescale is beyond the scope of this work.

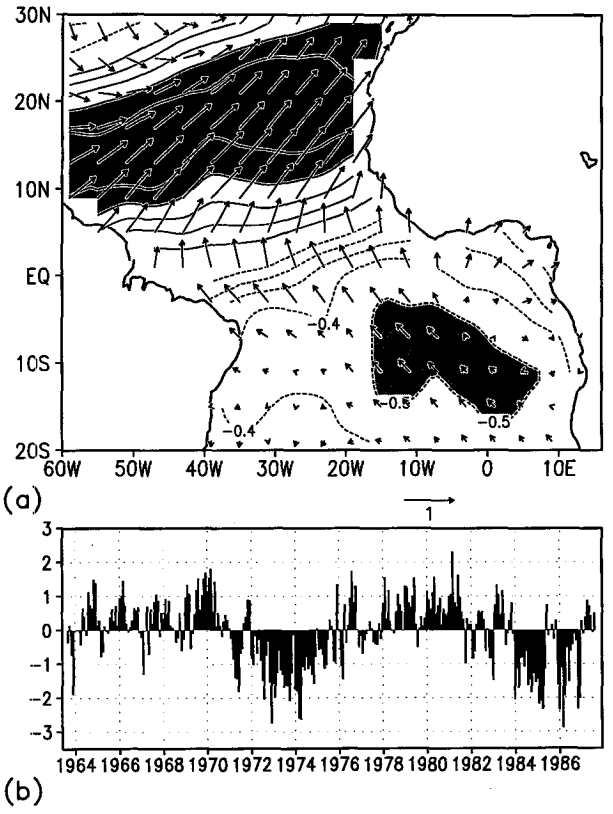

FIG. 2. The first joint EOF of SST, τ^X, and τ^Y monthly anomalies over the tropical Atlantic from September 1963 to August 1987; (a) the spatial pattern and (b) the associated coefficient time series. The contours represent the SST loadings; contour interval is 0.1; negative contours are dashed; values greater than 0.4 or lower than −0.5 are shaded; the zero contour is not drawn. The arrows represent the vectorial sum of τ^X and τ^Y loadings; the vectors are scaled accordingly to the arrow plotted at the lower right side of the upper panel.

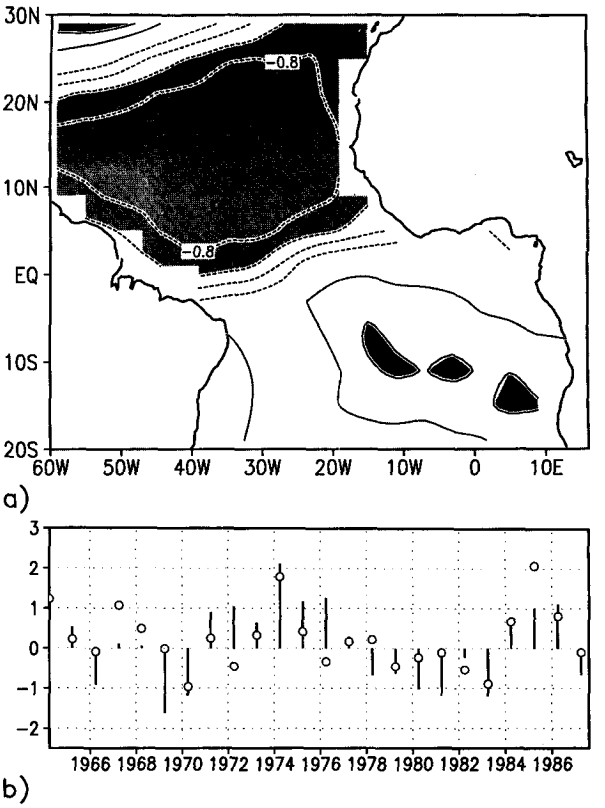

FIG. 3. The first EOF of MAM-only SST anomalies over the tropical Atlantic from 1964 to 1987; (a) the spatial pattern; contour interval is 0.2; negative contours are dashed; values greater than 0.4 or lower than −0.6 are shaded; the zero contour is not drawn; and (b) the associated coefficient time series (bars), and February–June rainfall departures over the northern Nordeste (open circles) (units of standard deviations, after C. A. Nobre 1995, personal communication).

Figure 3a shows the first EOF of MAM SST anomalies, which explains 31.8% of the variance after subtracting the annual cycle. It is noteworthy in Fig. 3a that amplitudes of the loadings over the northern tropical Atlantic are twice as large as those over southern Atlantic. The predominance of the anomalous SST pattern that is asymmetric relative to the equator, resembling a dipole, during MAM is consistent with the results of Hastenrath and Heller (1977), Hastenrath (1978), and Moura and Shukla (1981), which relates rainfall departures over the northern Nordeste with anomalous SST asymmetric relative to the equator over the tropical Atlantic during MAM.

The leading wind stress (joint τ^X and τ^Y) EOF over the tropical Atlantic is essentially the same as the one shown in Fig. 2a, but the maximum variance is explained by the DJF-only data sample (20.9%). Anom-

alous southeast and northeast trade winds are out of phase, albeit loadings are smaller over the southern than over the northern tropical Atlantic. This anomalous circulation pattern is consistent with the simultaneous weak North Atlantic subtropical high pressure cell and strong South Atlantic subtropical high pressure cell, and vice versa.

In summary, the leading joint SST, τ^x, and τ^y EOF (Fig. 2) presents clear evidence that a pattern of anomalous SST asymmetric relative to the equator is associated with anomalies of the trade winds over the tropical Atlantic, which also are asymmetric relative to the equator. Figure 2 also suggests that the pattern with north–south asymmetries of anomalous SST and stress is the most dominant mode of variability of the atmosphere–ocean system over the tropical Atlantic on interannual and longer timescales. The EOF results mentioned above are discussed in detail by Nobre (1993).

4. Composite analysis

We have utilized a simple compositing technique to study the time evolution of atmospheric and oceanic conditions over the tropical Atlantic. We have used the time series of the coefficients associated with the first eigenmode of SST anomalies shown in Fig. 3 as the basis to select the years for compositing. Also plotted in Fig. 3b is a rainfall index for the northern Nordeste region (C. A. Nobre 1995, personal communication). The compositing based on EOF amplitude is an appropriate procedure because it represents the entire pattern of anomalies. However, if the compositing were done using meridional SST gradients (Hastenrath and Greischar 1993), the outcome would be the same (not shown). This is so because the largest gradients tend to coincide with the occurrence of SST anomalies that are asymmetric relative to the equator.

The composite fields are calculated for the years in which the amplitude of the first EOF was either positive or negative, corresponding to the phase of the dipole pattern shown in Fig. 3 during MAM. So, each dataset is sorted into two subsets: one with the years in which the northern tropical Atlantic was colder than the mean, the southern tropical Atlantic warmer (called COLD cases: 1965, 1971, 1972, 1973, 1974, 1975, 1976, 1977, 1984, 1985, and 1986); the other with the years in which the SST anomaly pattern was reversed (called WARM cases: 1966, 1969, 1970, 1978, 1979, 1980, 1981, 1982, 1983, and 1987). Thus, the words COLD and WARM refer to SST anomalies in the northern tropical Atlantic. The time series of OLR, upper-tropospheric winds, and rainfall over the Atlantic start in June 1974; SLP ends in December 1985; and rainfall over South America ends in December 1984.

The COLD composites minus WARM composites (referred to as COLD − WARM) differences are presented throughout the text in order to emphasize the contrasts between COLD *and* WARM composites. Furthermore, since *each* COLD and WARM composite anomalous patterns are nearly the same in magnitude but opposite in sign, the COLD − WARM patterns shown in the following figures represent the average anomalous conditions for COLD composites, with magnitudes approximately doubled.

A remarkable aspect of Fig. 3b is the persistence of COLD SST pattern for seven years (1971 through 1977). For each of these seven years, rainfall over the northern Nordeste was above normal with the exception of 1972 and 1976, which were El Niño years. Although the length of data period is not adequate to make a definitive statement, it appears that there are decadal-scale variations of tropical Atlantic SST and northern Nordeste rainfall, which are only temporarily interrupted by El Niño. Mechanisms for the occurrence of such decadal-scale variations await explanation.

The statistical significance of the difference between COLD and WARM composites is done using the formula on Eq. (1) below, where it is assumed that the normalized difference on the right-hand side of the equation has a Student-t distribution of probabilities with $(n_c + n_w - 2)$ degrees of freedom:

$$t_{\alpha,(n_c+n_w-2)} \approx \frac{\langle x\rangle_c - \langle x\rangle_w}{\sqrt{n_c S_c^2 + n_w S_w^2}} \sqrt{\frac{n_c n_w (n_c + n_w - 2)}{n_c + n_w}}, \tag{1}$$

where $\langle x\rangle$ indicates the composite value of variable x; S is the standard deviation of $\langle x\rangle$; n is the number of cases used to compute $\langle x\rangle$; and the subscripts c and w refer to the COLD and WARM composites. Anomalies are accepted as statistically significant at the level of significance α (that is, the composite fields are statistically different from each other) if the right-hand side of Eq. (1) is greater than $t_{\alpha,(n_c+n_w-2)}$. The statistical significance of the composite differences are shown by shadings as indicated in the figures captions.

a. Sea surface temperature

Figure 4 shows the COLD − WARM composites of SST for DJF and MAM. During DJF (Fig. 4a), negative SST anomalies appear over the northeast Atlantic off the African coast; positive anomalies over the central South Atlantic. It is interesting to observe the apparent westward expansion of the anomalous SST over the northern tropical Atlantic from DJF to MAM (Fig. 4b). Though weaker, a similar westward expansion is also apparent over the southern tropical Atlantic in this figure (Markham and McLain 1977). The meridional gradient of anomalous SST is most intense during MAM, mainly because of the large SST anomalies over the northern tropical Atlantic. Also, it is worth mentioning that the interhemispherically asymmetric dipole pattern of SST anomalies during MAM (Fig. 4b) resembles the departure of seasonal (MAM) mean SST

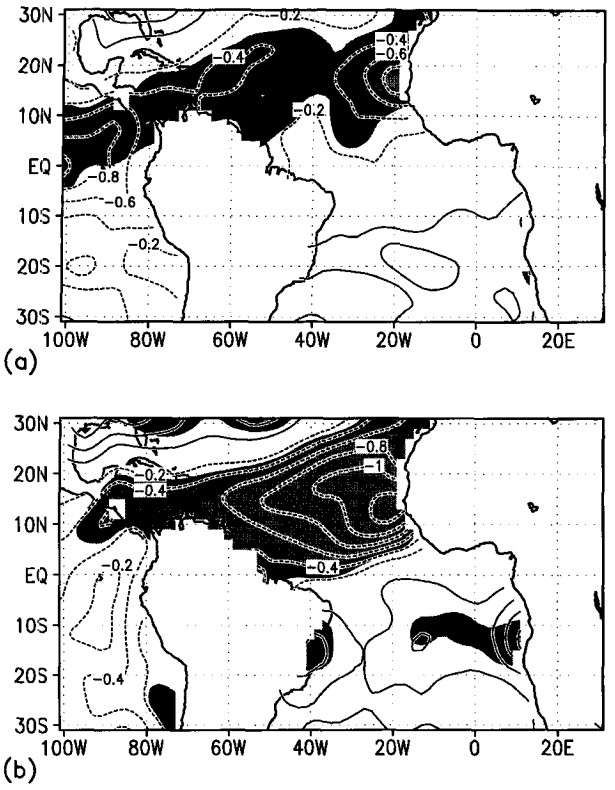

FIG. 4. COLD − WARM composite SST during (a) DJF and (b) MAM. Contour interval is 0.2°C. Negative contours are dashed. Shaded areas indicate anomalies statistically different from zero (t test) at 95% (heavy shade), 99% (medium shade), and 99.9% (light shade) significance levels.

from its annual mean over the tropical Atlantic (figure not shown). It indicates that SST interannual variability is modulated by the annual cycle of SST over the tropical Atlantic.

b. Wind stress

The COLD − WARM τ^y composite fields for DJF and MAM are shown in Fig. 5. During DJF (Fig. 5a), τ^y anomalies are generally small; largest anomalies appear over the northeast, southeast, and equatorial Atlantic. Taken together with the anomalous SST composite shown in Fig. 4a and the EOF results shown in Fig. 2, the τ^y anomalies over the northeast and southeast Atlantic during DJF are consistent with a possible forcing role of atmospheric circulation anomalies on the surface temperature of the ocean. Stronger northerlies enhance and weaker southerlies weaken upwelling of cold waters off the African coast, respectively, to the north and south of the equator.

During MAM (Fig. 5b), τ^y anomalies are stronger than during DJF, and the largest anomalies occur over the western equatorial Atlantic. The statistical significance of the composite fields are greater than 95% over the whole equatorial Atlantic, and significance reaches 99.9% at 5°N over western Atlantic. Coincidentally, MAM is the time when the meridional gradient of anomalous SST is strongest (Fig. 4b), so anomalous τ^y are directed toward the warmer waters and are strongest during MAM. It suggests that during MAM the wind stress anomalies are a response to the lower boundary forcing imposed by the meridional gradient of anomalous SST. Thus, Figs. 4 and 5 indicate the possibility of an interplay between atmospheric circulation anomalies and oceanic surface temperature. Modulations of the trade winds would force the distribution of anomalous SST during DJF, and then the atmospheric circulation would be forced by the meridional gradient of anomalous SST established during MAM, thus dislocating the intertropical convergence zone toward the anomalously warmer waters.

Figure 6 shows the COLD − WARM composite τ^x during DJF (Fig. 6a) and MAM (Fig. 6b). The τ^x anomalies are maximum during DJF, when they present a large-scale dipolelike configuration with negative anomalies to the north of the equator and positive anomalies to the south of the equator. During MAM, the τ^x dipole pattern is weaker and more narrowly confined to the equatorial region. The maximum of τ^x

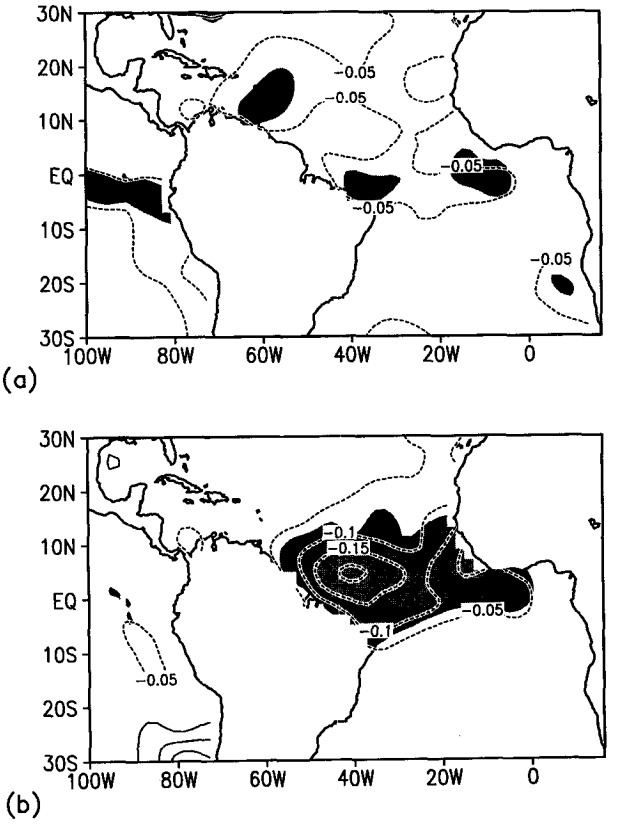

FIG. 5. As in Fig. 4 but for COLD − WARM composite τ^y during (a) DJF and (b) MAM. Contour interval is 0.05 dyn cm^{-2}.

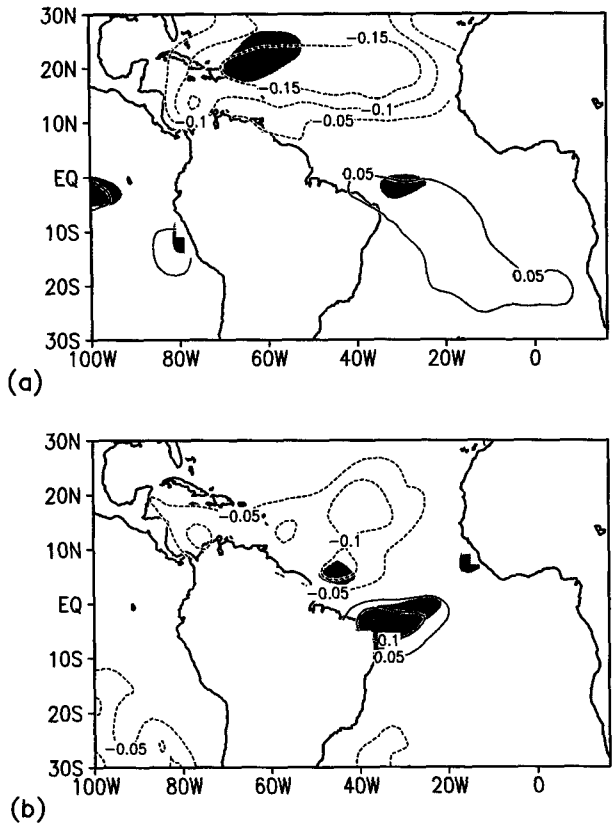

FIG. 6. As in Fig. 4 but for COLD − WARM composite τ^X during (a) DJF and (b) MAM. Contour interval is 0.05 dyn cm^{-2}.

composite anomalies during DJF contrasts with the SST and τ^y composites discussed above, which present the largest departures during MAM. Nevertheless, the statistical significance of τ^X composite differences shown in Fig. 6 is generally small.

The composite COLD − WARM wind stress fields for DJF and MAM are plotted in vectorial form in Fig. 7. The strong off-equatorial anomalies during DJF (Fig. 7a) and the strong cross-equatorial anomalies during MAM (Fig. 7b) are noteworthy. Furthermore, the MAM COLD − WARM composite shown in Fig. 7b is similar to MAM seasonal anomaly (departure from the annual mean) pattern of wind stress (figure not shown), indicating that interannual variability of surface wind stress over the equatorial Atlantic is phase locked with the annual cycle.

c. *Longitude–time cross sections*

Figure 8 shows longitude–time cross sections of SLP (averaged over 30°–40°N) and τ^X, τ^y, and SST (averaged over 10°–20°N) monthly COLD − WARM composites over the Atlantic. The largest anomalous τ^X (Fig. 8b) and τ^y (Fig. 8c) between 10°N and 20°N occur mostly from January through March and are concurrent with strong SLP anomalies farther north (Fig. 8a). Also, Fig. 8 reveals that while SLP presents a single maximum during February, τ^X (and to some extent also τ^y) has two maxima, one during January (at 35°W) and another during March (at 40°–45°W). These composites suggest the consistency between the pressure and wind fields.

Nevertheless, the strongest SLP and τ^X anomalies happen at approximately 40°W; the largest τ^y anomalies occur closer to the African coast between 20° and 35°W. This is consistent with an increased SLP over the North Atlantic and an associated increase of the atmospheric anticyclonic circulation. In addition, anomalous SSTs are maximum along the African coast during March and extend westward from January through April (Fig. 8d). The composite τ^y and SST longitude–time cross sections shown in Fig. 8 suggest the possibility of anomalous SSTs being locally induced by anomalous wind-driven upwelling off the African coast. Stronger τ^y generate Ekman drift currents at right angles to the wind, resulting in divergence in the surface layer of the ocean and stronger upwelling near the African shore. Similarly, the relaxation of τ^y locally generates warmer SSTs off the coast of Africa.

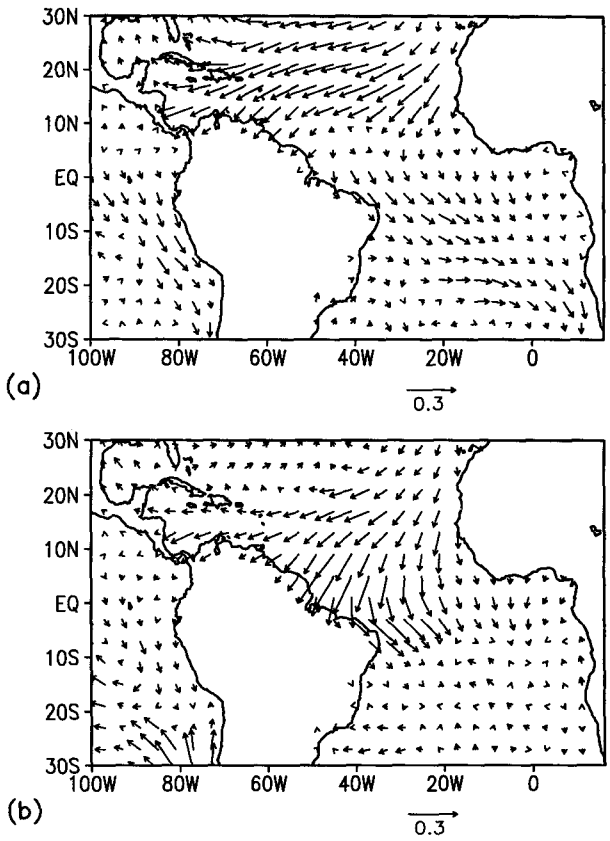

FIG. 7. COLD − WARM composite surface wind stress during (a) DJF, (b) MAM; the vector at the lower right corner of the figure represents 0.3 dyn cm^{-2}.

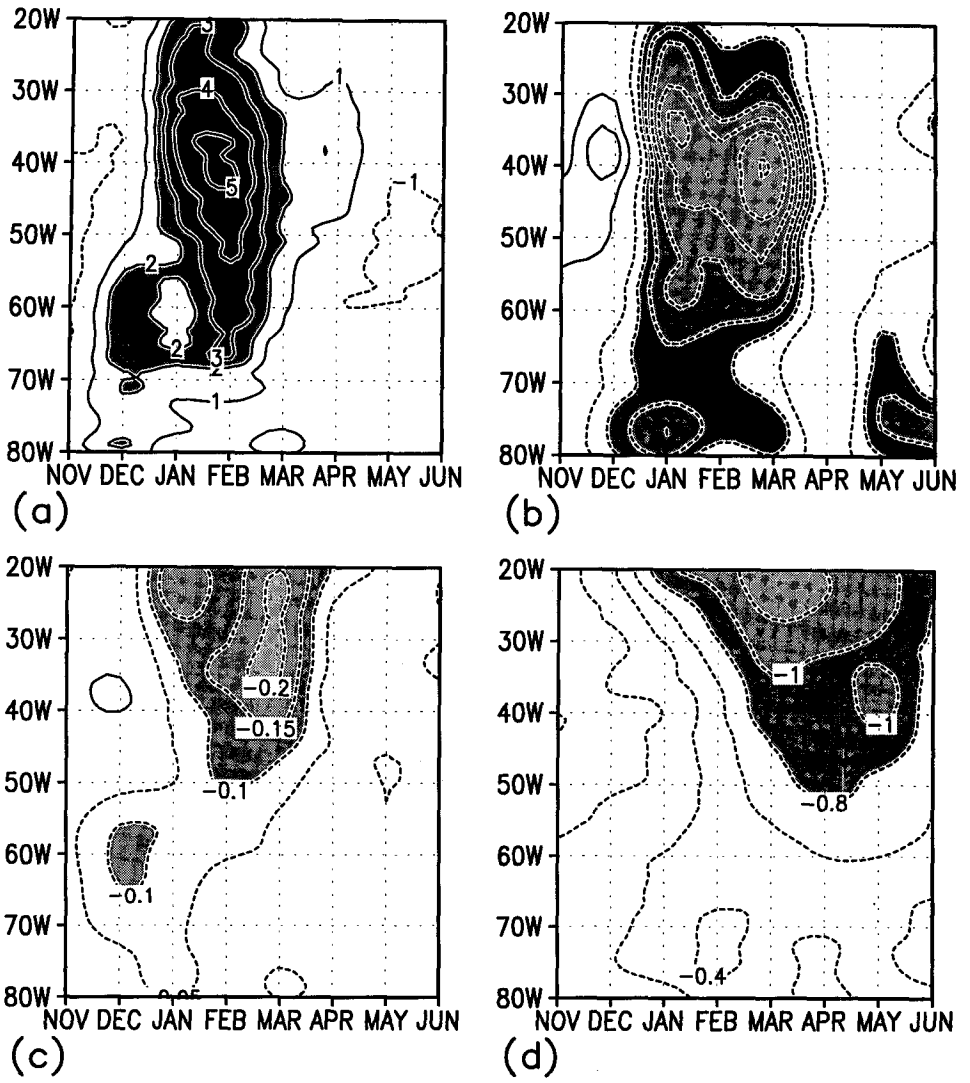

FIG. 8. COLD − WARM composite longitude–time cross sections over the tropical Atlantic of (a) SLP averaged over 30°–40°N, contour interval is 1 hPa, values greater than 2 hPa are shaded; (b) τ^x and (c) τ^y averaged over 10°–20°N, contour interval is 0.05 dyn cm^{-2}, values less than −0.1 are shaded; and (d) SST averaged over 10°–20°N, contour interval is 0.2°C., values less than −0.8 are shaded. Negative contours are dashed. Time ranges from November of the preceding years to June of the years chosen for compositing.

The apparent speed at which the composite anomalous SSTs expand westward from the African coast is approximately 10° per month (i.e., 0.4 m s^{-1}), as estimated from the slope of the −0.8°C isotherm from January to March in Fig. 8d.

Such westward expansion cannot be explained either by forced baroclinic Rossby waves or advection by wind-driven ocean currents. Winds that blow along a north–south oriented eastern shore can generate westward propagating Rossby waves (Anderson and Gill 1975; McCreary 1977; Philander and Yoon 1982). The wind-driven alongshore currents spread farther westward at lower latitudes (Carton and Philander 1984), where Rossby waves have higher phase speed. The fastest phase speed of a baroclinic Rossby wave (the first mode) at 15°N is approximately 0.1 m s^{-1}. Therefore, Rossby waves alone would not explain the observed westward expansion of the composite SST anomalies. If horizontal advection were the main mechanism, then warmer SST (associated with the weakening of the northeast trade winds) would not expand as far from the source region as the colder SST (associated with strengthening of the northeast trade winds). However, since both COLD and WARM composite anomalous SST do extend westward from the coast of Africa at about the same speed, it is not likely that advection plays a major role in this process.

Another possibility is the effect of wind-driven Ekman pumping over northern tropical Atlantic on the anomalous SST patterns locally. Carton and Philander (1984) suggested that for seasonal time scales, the curl of the wind is the dominant mechanism influencing the variability of currents in the interior part of the basin. Figure 9 shows January–March (JFM) time-averaged curl of the COLD – WARM composite wind stress. The positive anomalies between 5°N and 20°N generate horizontal divergence on the surface layer of the ocean and upwelling. Therefore, Fig. 9 suggests there would be upwelling over the central northern Atlantic between 10° and 20°N during January–March. However, the strongest SST anomalies over that area are observed during March–April. Thus, we speculate the apparent westward expansion of anomalous SST over the northern tropical Atlantic may be a consequence of the combined effects of upwelling and direct atmospheric forcing. The deeper the thermocline, the longer it would take for upwelled waters to affect SST. Since the thermocline is deeper in the western Atlantic than in the eastern Atlantic (Philander 1990), SST anomalies would take longer to appear over the western than the eastern tropical Atlantic.

Another important aspect of the COLD *and* WARM composites of τ^x, τ^y, and SLP over the northern tropical Atlantic is that they differ from the climatology only during JFM. This can be seen clearly in Fig. 10, which shows the time evolution of the area-averaged COLD composites, WARM composites, and climatology over the northern tropical Atlantic. SLP (Fig. 10a) and wind stress (Figs. 10b,c) composites differ from the climatology during JFM starting abruptly in January, whereas SST (Fig. 10d) composites differ from the climatology only after February. A Monte Carlo technique was used to assess the statistical significance of the departures from the climatology shown in Fig. 10. One hundred composites with ten years chosen at random were calculated for each month from September to August. The standard deviation among the random composites were computed. The differences COLD – WARM for SLP during January and February represent approximately 2.3 standard deviations of the random SLP composites, τ^x and τ^y differences from January to March are between 3.0 and 4.0 standard deviations, while SST differences during March and April are greater than 6.0 standard deviations of the respective random composites.

The results shown in Fig. 10 suggest that the COLD and WARM composites over northern Atlantic (between 10° and 40°N) are distinct, with anomalies of opposite sign, during only a few months preceding the MAM season. On the other hand, COLD and WARM SST composites over the tropical Atlantic and τ^y composites over the equatorial Atlantic (figure not shown) present distinct patterns from February to June.

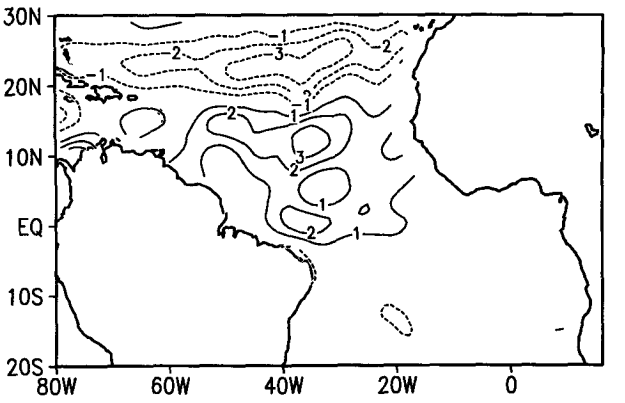

FIG. 9. COLD – WARM composite surface wind stress curl during January–February–March. Units are 10^{-8} dyn cm^{-3}. Negative contours are dashed.

d. *Intertropical convergence zone*

The differences of ITCZ positions for the years in which the anomalous SST dipole patterns show the COLD phase or the WARM phase during MAM have dramatic implications for the rainfall distribution over northern Nordeste. The rainy season over northern Nordeste is centered in March, coinciding with the period of climatological southernmost displacement of the ITCZ (Hastenrath and Heller 1977). Figure 11 shows a latitude–time cross section of confluence axis ($\tau^y = 0$) as a measure of the ITCZ position at longitude 30°W for the COLD and WARM composites and for the climatology. The months used in the stratification process are MAM. From September through January there is practically no difference among the ITCZ positions for each of the composites and the climatology. After January, however, the ITCZ remains north of its climatological positions for the WARM composites and south for the COLD composites. The maximum displacement, either to the north (for the WARM composites) or to the south (for the COLD composites), occurs in April. Coincidentally, the meridional gradient of composite anomalous SSTs is maximum between March and May (Fig. 4b). Also, the ITCZ reaches the southernmost latitudes during March for the WARM composites and for the climatology, while for the COLD composite the ITCZ remains south of the equator until April. As a consequence, rainfall to the south of the equator is more abundant during the COLD composites because of the extended period for which the ITCZ remains to the south of its normal position organizing deep cumulus convection.

e. *Rainfall*

The contrast described above is further illustrated in Fig. 12, which shows the area-averaged WARM and COLD composite anomalous monthly precipitation

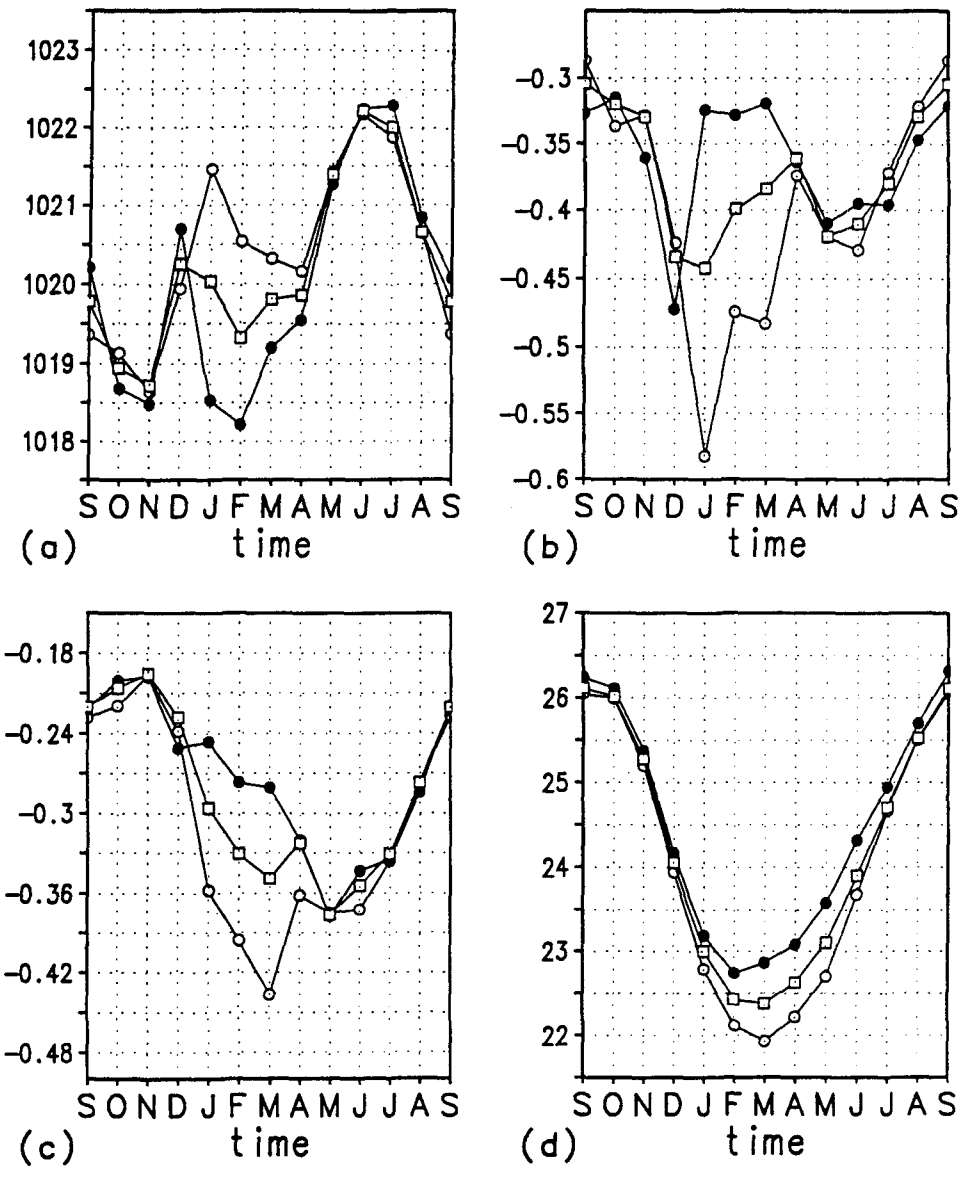

FIG. 10. Time series of area averaged (40°–20°W) (a) SLP over 20°–40°N, and (b) τ^x, (c) τ^y, and (d) SST over 10°–30°N; WARM composites (full circles), COLD composites (open circles), and climatology (open squares) from September of the preceding years to September of the years chosen for compositing.

over the northern Nordeste, eastern Amazon, and southern Nordeste areas (see map in Fig. 1) from September through August. The main differences between the WARM and COLD composites for the northern Nordeste (Fig. 12a) and eastern Amazon (Fig. 12b) are the intensity and duration of the rainy season over those areas. For the WARM cases (dark bars), precipitation is less abundant than the mean, and the maximum rainfall coincides with the climatological maximum rainfall (during March) over both Nordeste and eastern Amazon. For the COLD cases (open bars), the maximum rainfall occurs in April and the rainfall volume during and after the rainy season is larger than for the WARM case. This suggests that a wetter than normal year over the northern Nordeste and eastern Amazon is an outcome of both an increased rate of precipitation during the rainy season and an extended duration of the period of rain. This is consistent with the observed positions of the ITCZ for the WARM and COLD composites shown in Fig. 11. The similarities between the temporal distribution of rainfall over the northern Nordeste and eastern Amazon discussed above suggest that the precipitation anomalies affecting Nordeste are part of a large-scale phenomenon encom-

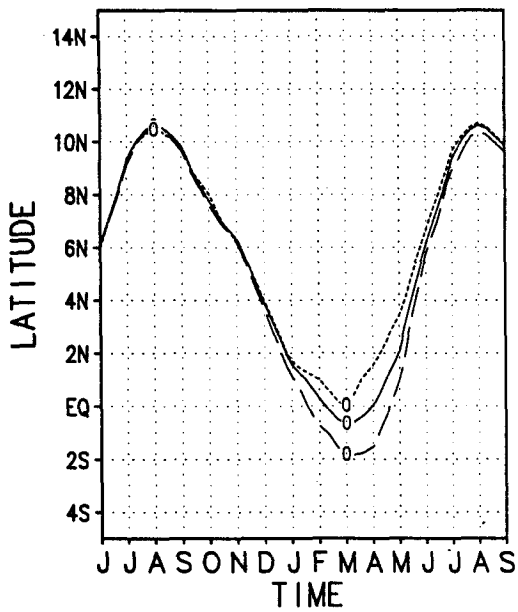

FIG. 11. The meridional displacement of the ITCZ (i.e., the position where $\tau^y = 0$) at longitude 30°W over the tropical Atlantic for the WARM composites (short-dashed line), COLD composites (long-dashed line), and the climatology (continuous line). Time ranges from June of the preceding years to September of the years chosen for compositing.

passing the whole region covering the northern Nordeste and eastern Amazon.

The area average of composite rainfall over the southern Nordeste (Fig. 12c) shows wet years associated with the COLD composites and dry years associated with WARM composites. Also, dry years are characterized by the absence of the climatological maximum rainfall during DJF. Maximum rainfall occurs in January for the wet years, whereas two secondary maxima occur in November and March during dry years. A large fraction of the total rainfall over southern Nordeste, which falls mostly during December and January, is due to the penetration of baroclinic frontal systems from higher latitudes of the Southern Hemisphere (Kousky 1979). It is possible that middle latitude atmospheric dynamics, as well as the planetary-scale atmospheric anomalies induced by ENSO over the tropical Pacific (Bjerknes 1969; Ropelewski and Halpert 1987), play an important role in the rainfall distribution over southern Nordeste.

Figure 13 shows the spatial distribution of COLD − WARM composites during DJF (Fig. 13a) and MAM (Fig. 13b). The out of phase rainfall distribution over southern Nordeste during DJF and northern Nordeste during MAM is apparent. During MAM of the years in which northern tropical Atlantic is colder than normal and southern tropical Atlantic is warmer than normal, the band of maximum rainfall associated with the ITCZ is displaced southward, resulting in the pattern in Fig. 13b. The westward extension of positive anomalies into the Amazon region is noteworthy. The northward shift of the ITCZ is associated with the years in which SST anomalies show the reverse phase (Hastenrath and Heller 1977; Moura and Shukla 1981). However, during DJF (Fig. 13a) there is also a pattern of anomalous rain, which is asymmetric about the equator and has its centers farther north and south from the equator.

The large-scale pattern of rainfall anomalies over northern South America is illustrated better when both the WARM and COLD composite rainfall anomalies are plotted separately for each station (Fig. 14). The symbols plotted in Fig. 14 represent five classes of composite rainfall anomalies normalized by the local standard deviation. During DJF, the COLD composite (Fig. 14a) shows negative anomalies throughout the southern Nordeste and positive anomalies over the cen-

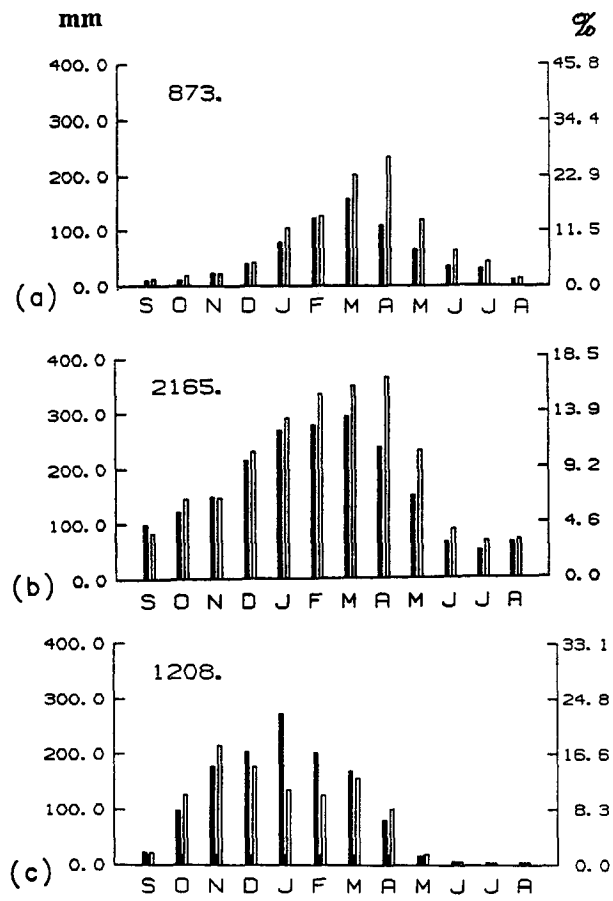

FIG. 12. Monthly composite rainfall over (a) northern Nordeste, (b) eastern Amazon, and (c) Southern Nordeste (see localization map in Fig. 1) for the WARM composites (dark bars) and COLD composites (open bars). Time ranges from September of the preceding years to August of the years chosen for compositing. Annual total rainfall (mm) for each area is indicated in the upper left corner of each panel.

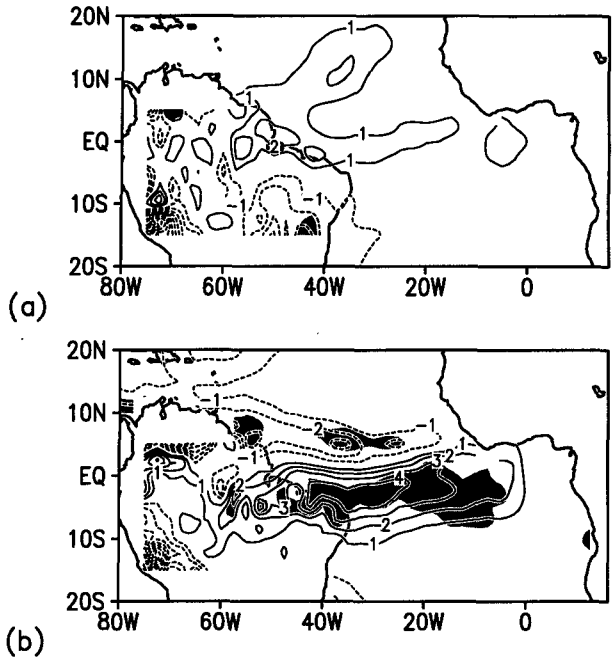

FIG. 13. Same as in Fig. 4 but for COLD − WARM composite rainfall over the tropical Atlantic and northern South America during (a) DJF and (b) MAM. Contour interval is 1 mm day^{-1}.

tral and northern Amazon region. The WARM composite relative to DJF (Fig. 14c) shows an anomalous rainfall pattern that is nearly the reverse of the COLD composite for the same period (Fig. 14a). During MAM, the COLD composite (Fig. 14b) shows positive rainfall anomalies over the Amazon and northern Nordeste; the WARM composite (Fig. 14d) shows a reverse pattern, with negative anomalies over the Amazon and northern Nordeste. Thus, Fig. 13 and Fig. 14 indicate clearly that the precipitation anomalies that affect north-northeastern Brazil during the years in which anomalous SST dipole patterns are present in the Atlantic are part of a large-scale anomalous rainfall pattern. Also, the composite rainfall anomalies over southern Nordeste during DJF have opposite sign as those over the northern Nordeste and eastern Amazon during MAM. This result is particularly relevant since DJF encompasses the rainy season over southern Nordeste; MAM over northern Nordeste.

f. Teleconnections

It is of interest to investigate whether or not remotely forced atmospheric disturbances might be contributing to explain the interannual climate variability over the tropical Atlantic. Figure 15 shows SLP and the 200-hPa zonal wind composite COLD − WARM differences during JFM. Teleconnection patterns between the Pacific and the North Atlantic are suggested in Fig. 15. The strong SLP anomalies over the northern Pacific and Atlantic basins (Fig. 15a), both of them statistically significant at the 95% level, are consistent with the signature of the Pacific–North America (PNA) teleconnection pattern at the surface (Horel and Wallace 1981). Since the center over the southeastern United States projects partially into the northern Atlantic subtropical ridge, ENSO warm events could favor lower SLP over the North Atlantic (and the cold phase of ENSO would favor higher SLP). The pattern of these composites remains unchanged even if we eliminated the strong ENSO of 1982–83.

On the other hand, results of previous works show that SLP over the South Atlantic is negatively correlated with the Southern Oscillation (Hastenrath et al. 1987; Aceituno 1988; Chu 1991; Hameed et al. 1993) (e.g., the warm phase of ENSO would be associated with an increase of SLP over the South Atlantic). Therefore, it is plausible to conjecture that out-of-phase SLP anomaly patterns over the northern and southern Atlantic may be induced, in part, by global-scale anomalous circulation patterns associated with ENSO.

The 200-hPa COLD − WARM composite zonal wind for JFM (Fig. 15b) shows a pattern over the central Pacific and equatorial Atlantic that resembles the pattern observed during the cold phase of ENSO (Kousky and Kayano 1994). Also, the circulation pattern in Fig. 15b indicates the existence of an upper-tropospheric trough over the southern Nordeste, which causes subsidence and inhibits the development of deep cumulus clouds. Teleconnections from the equatorial Pacific into higher latitudes of the Southern and Northern Hemispheres are also suggested in Fig. 15b. The baroclinic vertical structure of the anomalous wind composites over the equatorial Pacific and Atlantic, as well as the equivalent barotropic structure over North Pacific and North Atlantic, is shown in the height–latitude cross sections of the COLD − WARM composite zonal wind during JFM (Fig. 16). The teleconnection patterns suggested in Figs. 15 and 16 (Hoskins and Karoly 1981) are an indication of the possible role of Tropics–extratropics interactions in affecting atmospheric circulation over the Atlantic, which in turn modulates SST anomalous patterns over the tropical Atlantic.

It is to be noted that the composite patterns in Figs. 15 and 16, based solely on the hemispherically asymmetric dipole pattern of anomalous SST over the tropical Atlantic, show distinctive ENSO characteristics over the Pacific and the Atlantic as discussed above. However, it remains to be reconciled that there is markedly low frequency variability over the tropical Atlantic that cannot be accounted for by ENSO variability.

g. Outgoing longwave radiation

A further indication of the role of ENSO on the interannual variability of the atmosphere over the tropical Atlantic is given by the COLD − WARM OLR com-

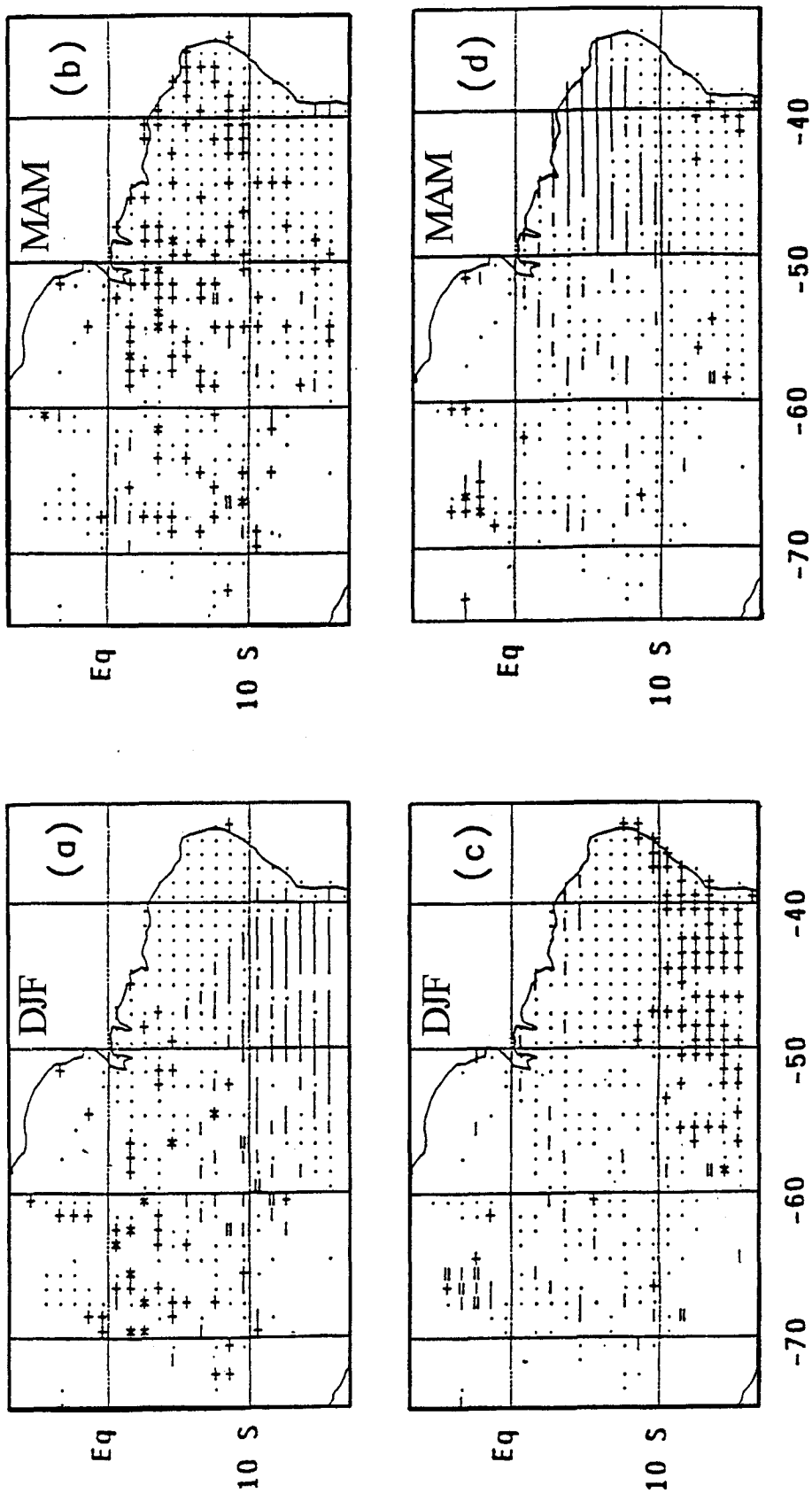

FIG. 14. Composite rainfall departures (station data) from the long-term mean normalized by the local standard deviation over northern Brazil for COLD composites during (a) DJF and (b) MAM and WARM composites during (c) DJF and (d) MAM. The symbols plotted on the map represent rainfall departures in units of standard deviations: less than −1.5 "="; between −1.5 and −0.5 "−"; between −0.5 and 0.5 "."; between 0.5 and 1.5 "+"; greater than 1.5 "*".

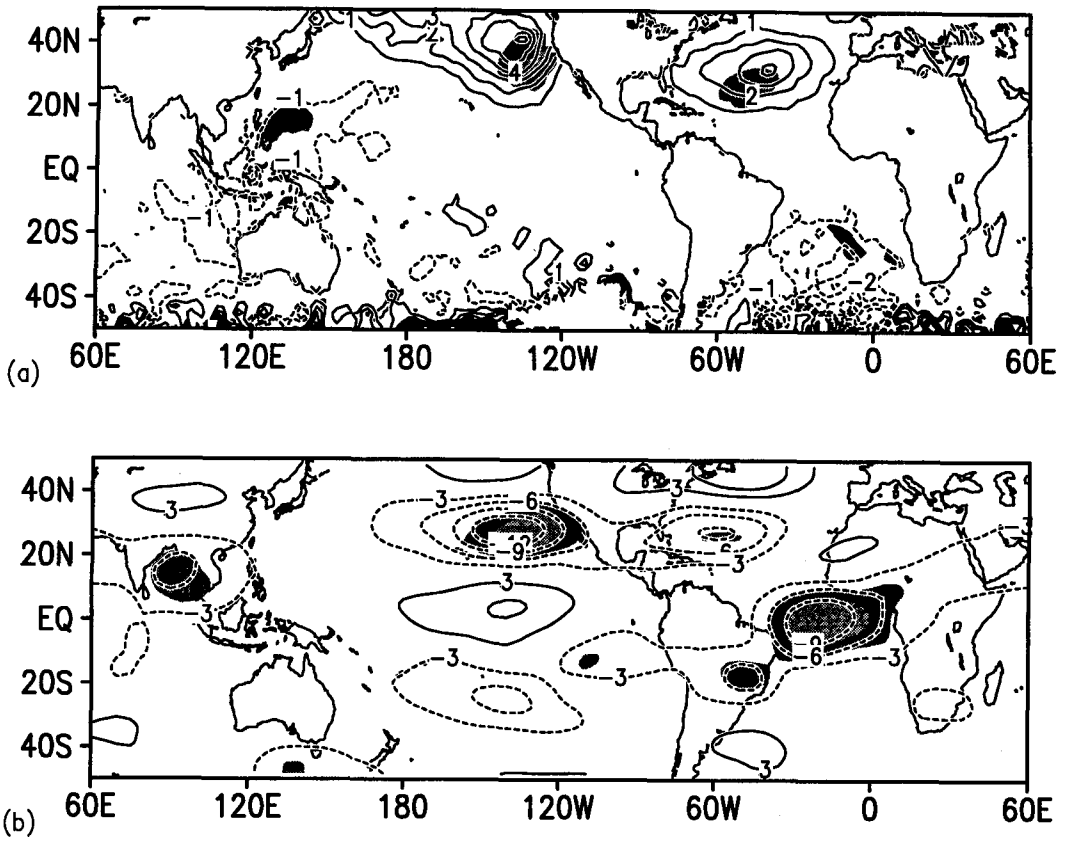

FIG. 15. As in Fig. 4 but for JFM COLD − WARM composite (a) SLP, contour interval is 1 hPa, and (b) 200-hPa zonal wind, contour interval is 3 m s^{-1}.

posites shown in Fig. 17. During the September–November (SON) composite (Fig. 17a) there is increased convection over Indonesia and reduced convection over the date line; the south Pacific convergence zone (SPCZ) is displaced westward. During DJF (Fig. 17b), positive OLR anomalies (reduced convection) over the central equatorial Pacific expand eastward; a dipole pattern over the tropical Atlantic depicts positive anomalies over the southwest tropical Atlantic and negative anomalies over the northeast. During MAM (Fig. 17c), positive OLR anomalies expand farther eastward across the equatorial Pacific; the ITCZ over the Atlantic is displaced southward. The time evolution of the anomalous OLR pattern over the Pacific, as inferred from Fig. 17, resembles anomalous OLR patterns associated with the cold phase of ENSO. Over the Atlantic, the asymmetric anomalous OLR patterns about the equator during DJF and MAM are consistent with the anomalous rainfall patterns shown in Fig. 13. Furthermore, there is an apparent relationship between OLR and SST anomalies over the tropical Atlantic. During DJF, higher rainfall and convection (i.e., decreased OLR) occurs over the northern tropical Atlantic, perhaps further reducing the incoming radiation to the ocean surface and further cooling the ocean surface. We do not know quantitatively how important this effect is in changing SST.

5. Conclusions

EOF analyses were used to identify objectively the dominant modes of sea surface temperature and wind stress interannual variability over the tropical Atlantic. The EOF results shown in the present study suggest that interannual variability of SST and surface wind stress over the tropical Atlantic is dominated by a pattern asymmetric relative to the equator. In agreement with previous works, weaker trade winds are associated with warmer SST and stronger trade winds with cooler SST. The leading eigenvectors of both the zonal component of the wind stress anomalies during DJF and SST anomalies during MAM present patterns that are also asymmetric relative to the equator. These are the seasons when the time variance of wind stress and SST are maximum over the northern tropical Atlantic. The leading eigenvector of the meridional component of the

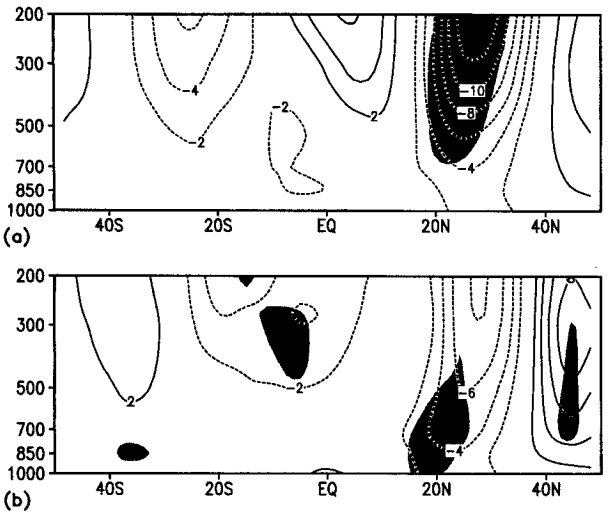

FIG. 16. As in Fig. 4 but for latitude–height cross sections of JFM COLD – WARM composite zonal wind averaged over longitudes (a) 160°–120°W and (b) 70°–30°W. Contour interval is 2 m s^{-1}; negative contours are dashed.

wind stress anomalies shows maximum amplitude over the western equatorial Atlantic during MAM and points from the hemisphere of cooler SST to the warmer SST. Furthermore, the time variance explained by the EOFs over the northern tropical Atlantic is twice as much as over the southern tropical Atlantic.

SST anomalies form off the African coast as a result of anomalous wind stresses along the coast during January and extend westward during the following two to three months. This westward expansion of anomalous SST are most noticeable over the northern tropical Atlantic. The largest SST anomalies in the interior of the basin occur during March–April. We speculate that cooling (warming) near the coast is related to local upwelling (donwelling) (Nykjær and Van Camp 1994), whereas cooling (warming) in the interior is caused mainly by evaporation due to stronger (weaker) trade winds. The apparent westward expansion of the composite anomalous SST would then be explained by the combined effects of upwelling and evaporation.

The results of the composite analyses suggest that variations in the strength of the trade winds appear as a primary forcing for the thermal changes in the upper ocean over the tropical Atlantic, resulting in the anomalous SST dipole patterns. On the other hand, the meridional component of the wind appears to be in response to the anomalous meridional gradients of SST over the equatorial Atlantic. It is suggested that atmospheric circulation anomalies over off-equatorial tropical Atlantic first force the formation of anomalous SST meridional gradient, which in turn forces the ITCZ to be displaced toward warmer waters, thus affecting the rainfall distribution over the equatorial Atlantic and adjoining land areas. It is shown that precipitation anomalies linked to anomalous displacements of the ITCZ are basinwide, extending over the northern Nordeste and eastern Amazonia. Therefore, the known droughts over the Nordeste are part of continental-scale precipitation anomalies.

This work has brought further observational evidence that in addition to a northward shift of the ITCZ during MAM of the years in which the meridional gradient of anomalous SST is directed north (and southward in the years in which the meridional gradient of anomalous SST points to the south), the principal reason for the rainfall deficiency (excess) over the northern Nordeste and eastern Amazonia is the early (latter) withdrawal of the ITCZ toward the Northern Hemisphere. The northward displacement of the ITCZ over the western Atlantic starts in March when the northern tropical Atlantic is warmer than normal; however, when the southern tropical Atlantic is warmer than normal, the ITCZ begins to move northward during April. Accordingly, composite rainfall over the northern Nordeste and eastern Amazon show the largest differences between wet and dry years in April.

Also, it is suggested that the atmospheric teleconnection pattern associated with ENSO over the equatorial Pacific influences the formation of meridional gradient of anomalous SST over the equatorial Atlantic. Previous literature has shown evidence of an ENSO-related east–west anomalous circulation cell between the equatorial eastern Pacific and the equatorial and South Atlantic. This paper brings evidence that teleconnection patterns propagating from the equatorial Pacific into higher latitudes of the Northern Hemisphere (e.g., the PNA pattern) induce SLP anomalies of the opposite sign over the northern tropical Atlantic. Once SLP anomalies of opposite sign are set over the northern and southern Atlantic, then hemispherically asymmetric trade winds and SST anomalies follow, as suggested from the composite analyses in this paper.

Though composite SST and wind stress anomalies over the northern tropical Atlantic shown in this paper are twice as large as those over the southern tropical Atlantic, there is a tendency for the composite anomalous SST and wind stress over the southern and northern tropical Atlantic to be out of phase, characterizing what is referred to in the literature as the dipole pattern of anomalous SST. This asymmetry was also apparent in the EOF analyses done in this study.

Composite SLP and both surface wind stress and tropospheric winds over the North Atlantic are strongly locked to the annual cycle. They depart from the climatology only during JFM. SST composites over the tropical Atlantic and meridional component of the wind stress over the equatorial Atlantic differ from the climatology from February through June. However, anomalous patterns of upper-level winds and OLR over the equatorial belt can be detected as early as September.

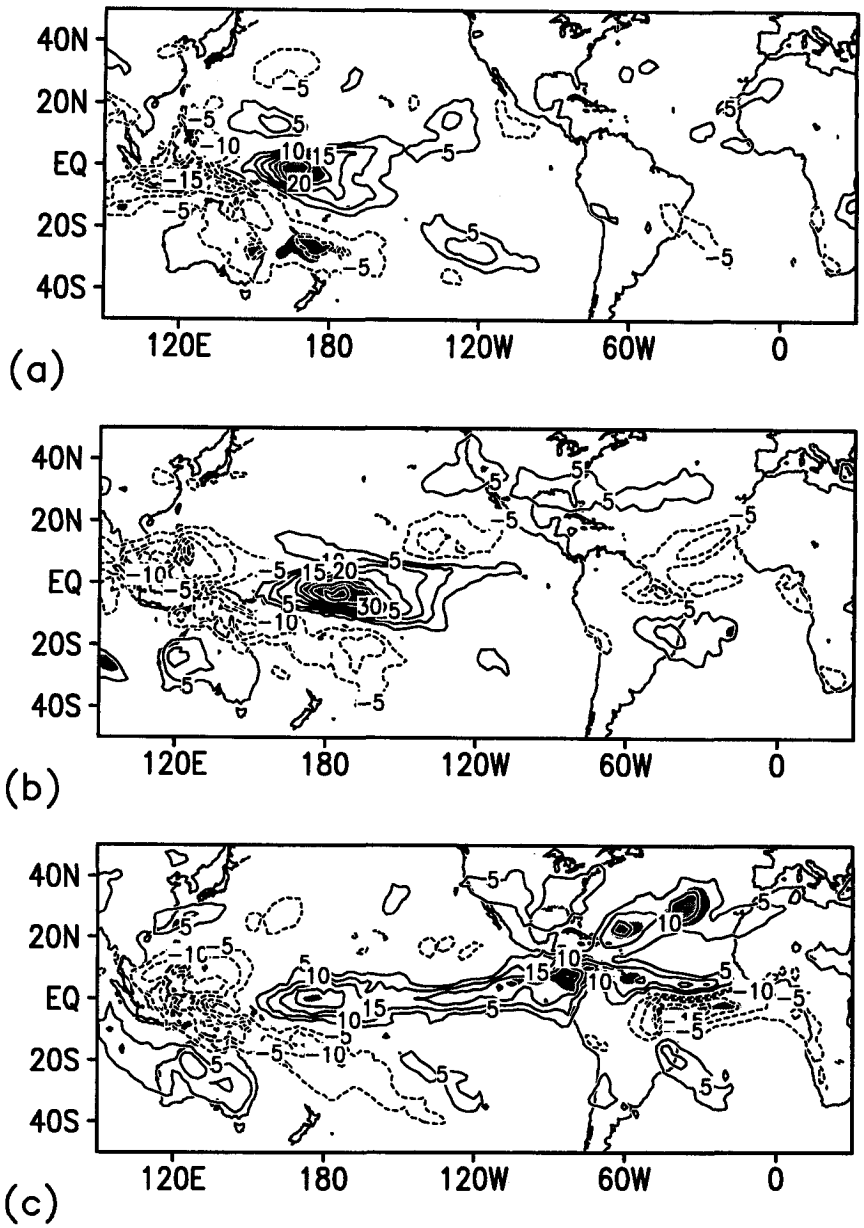

FIG. 17. As in Fig. 4 but for COLD − WARM composite OLR during (a) SON, (b) DJF, and (c) MAM. Contour interval is 5 W m^{-2}.

This study suggests that the anomalous rainfall patterns that affect north-northeastern Brazil are the result of a sequence of phenomena that evolve during several months and encompass both the Pacific and the Atlantic Oceans. The ideas presented here can be readily tested using coupled ocean–atmosphere models.

Acknowledgments. The first author express his gratitude to the colleagues at COLA with whom he had the opportunity to work. Special thanks are given to Dr. P. A. Dirmeyer, Dr. B. Huang, Dr. V. E. Kousky, and Mr. L. Marx for helpful discussions. The reviewers of this paper are thanked for their valuable comments and suggestions. This research was supported by NSF Grant ATM-9019296 and NASA Grant NAGW-557.

REFERENCES

Aceituno, P., 1988: On the functioning of the Southern Oscillation in the South American sector. Part 1: Surface climate. *Mon. Wea. Rev.*, **116,** 505–524.

Anderson, D. L. T., and A. E. Gill, 1975: Spin-up of a stratified ocean, with applications to upwelling. *Deep-Sea Res.*, **22,** 583–596.

Arkin, P. A., 1982: The relationship between interannual variability in the 200 mb tropical wind field and the Southern Oscillation. *Mon. Wea. Rev.*, **110,** 1393–1404.

Bjerknes, J., 1969: Atmospheric teleconnections from the equatorial Pacific. *Mon. Wea. Rev.*, **97,** 526–535.

Carton, J. A., and S. G. H. Philander, 1984: Coastal upwelling viewed as a stochastic phenomenon. *J. Phys. Oceanogr.*, **14,** 1499–1509.

——, and B. Huang, 1994: Warm events in the tropical Atlantic. *J. Phys. Oceanogr.*, **24,** 888–903.

Chu, P. S., 1991: Brazil's climate anomalies and ENSO. *Teleconnections Linking Worldwide Climate Anomalies,* M. H. Glantz, R. W. Katz, and N. Nicholls, Eds., Cambridge University Press, 43–71.

Curtis, S., and S. Hastenrath, 1995: Forcing of anomalous sea surface temperature evolution in the tropical Atlantic during Pacific warm events. *J. Geophys. Res. Oceans,* **100,** 15 835–15 847.

Dirmeyer, P. A., and J. Shukla, 1993: Observational and modeling studies of the influence of soil moisture anomalies on atmospheric circulation (review). *Prediction of Interannual Climate Variations,* J. Shukla, Ed., NATO ASI Series, 1–23.

Halpert, M. S., and C. F. Ropelewski, 1989: *Atlas of Tropical Sea Surface Temperature and Surface Winds.* U.S. Department of Commerce, NOAA Atlas No. 8, 164 figures, 14 pp.

Hameed, S., K. R. Sperber, and A. Meinster, 1993: Teleconnections of the Southern Oscillation in the tropical Atlantic sector in the OSU coupled upper ocean–atmosphere GCM. *J. Climate,* **6,** 487–498.

Hastenrath, S., 1978: On modes of tropical circulation and climate anomalies. *J. Atmos. Sci.,* **35,** 2222–2231.

——, 1984: Interannual variability and annual cycle: Mechanisms of circulation and climate in the tropical Atlantic. *Mon. Wea. Rev.,* **112,** 1097–1107.

——, and L. Heller, 1977: Dynamics of climatic hazards in northeast Brazil. *Quart. J. Roy. Meteor. Soc.,* **110,** 77–92.

——, and L. Druyan, 1993: Circulation anomaly mechanisms in the tropical Atlantic sector during the Northeast Brazil rainy season. *J. Geophys. Res. Atmos.,* **98,** 14 917–14 923.

——, and A. Greischar, 1993: Circulation mechanisms related to Northeast Brazil rainfall anomalies. *J. Geophys. Res. Atmos.,* **98,** 5093–5102.

——, L. C. Castro, and P. Aceituno, 1987: The Southern Oscillation in the tropical Atlantic sector. *Contrib. Atmos. Phys.,* **60,** 447–463.

Horel, J. D., and M. J. Wallace, 1981: Planetary-scale atmospheric phenomena associated with the southern oscillation. *Mon. Wea. Rev.,* **109,** 813–829.

Hoskins, B. J., and D. J. Karoly, 1981: The steady linear response of a spherical atmosphere to thermal orographic forcing. *J. Atmos. Sci.,* **38,** 1179–1196.

Huang, B., 1992: A numerical simulation of the seasonal and interannual variability of the tropical Atlantic circulation with a general circulation model of the ocean. Ph.D. thesis, University of Maryland, 210 pp.

Kousky, V. E., 1979: Frontal influences on Northeast Brazil. *Mon. Wea. Rev.,* **107,** 1140–1153.

——, and M. T. Kayano, 1994: Principal modes of outgoing longwave radiation and 250-mb circulation for the South American sector. *J. Climate,* **7,** 1131–1143.

Kutzbach, J. E., 1967: Empirical eigenvectors of sea-level pressure, surface temperature and precipitation complexes over North America. *J. Appl. Meteor.,* **6,** 791–802.

Lamb, P. J., 1978a: Case studies of tropical Atlantic surface circulation patterns during recent subsaharan weather anomalies: 1967 and 1968. *Mon. Wea. Rev.,* **106,** 482–491.

——, 1978b: Large-scale tropical Atlantic surface circulation patterns associated with Subsaharan weather anomalies. *Tellus,* **30,** 240–251.

Lough, J. M., 1986: Tropical Atlantic sea surface temperatures and rainfall variations in Subsaharan Africa. *Mon. Wea. Rev.,* **114,** 561–570.

Markham, C. G., and D. R. McLain, 1977: Sea surface temperature related to rain in Ceara, northeastern Brazil. *Nature,* **265,** 320–325.

McCreary, J. P., 1977: Eastern ocean response to changing wind systems. Ph.D. thesis, University of California at San Diego, 156 pp.

Merle, J. M. F., and P. Hisard, 1980: Annual signal and interannual anomalies of sea surface temperature in the eastern equatorial Atlantic Ocean. *Deep-Sea Res.,* **26,** 77–101.

Moura, A. D., and J. Shukla, 1981: On the dynamics of droughts in northeast Brazil: Observations, theory and numerical experiments with a general circulation model. *J. Atmos. Sci.,* **38,** 2653–2675.

Nobre, P., 1993: On the genesis of anomalous SST and rainfall patterns over the tropical Atlantic basin. Ph.D. dissertation, University of Maryland at College Park, 151 pp.

——, and J. Shukla, 1991: Interannual variability of SST and wind stress over the tropical Atlantic and rainfall over Amazon and Northeast Brazil. Preprints, *Fifth Conf. on Climate Variations,* Vol. 1, Denver, CO, Amer. Meteor. Soc., 472–475.

Nykjær, L., and L. Van Camp, 1994: Seasonal and interannual variability of coastal upwelling along northwest Africa and Portugal from 1981 to 1991. *J. Geophys. Res.,* **99,** 14 197–14 207.

Palmer, T. N., 1986: Influence of the Atlantic, Pacific and Indian Oceans on Sahel rainfall. *Nature,* **322,** 251–253.

Parish, D. F., and R. E. Kistler, 1982: Evolution of the NMC data assimilation system: September 1978–January 1982. *Mon. Wea. Rev.,* **110,** 1335–1346.

Parker, D. E., C. K. Folland, and M. N. Ward, 1988: Sea surface temperature anomaly patterns and prediction of seasonal rainfall in the Sahel region of Africa. *Nature,* **310,** 483–485.

Philander, S. G. H., 1990: *El Niño, La Niña, and the Southern Oscillation.* Academic Press, 293 pp.

——, and J.-H. Yoon, 1982: Eastern boundary currents and coastal upwelling. *J. Phys. Oceanogr.,* **12,** 862–879.

——, and R. C. Pacanowski, 1986: A model of the seasonal cycle in the tropical Atlantic Ocean. *J. Geophys. Res.,* **91,** 14 192–14 206.

Ropelewski, C. F., and M. S. Halpert, 1987: Global and regional scale precipitation patterns associated with the El Niño/Southern Oscillations. *Mon. Wea. Rev.,* **115,** 1606–1626.

Servain, J. M., 1991: Simple climatic indices for the tropical Atlantic Ocean and some applications. *J. Geophys. Res.,* **96,** 15 137–15 146.

Shukla, J., 1984: Predictability of time averages: Part II: The influence of the boundary forcings. *Problems and Prospects in Long and Medium Range Weather Forecasting,* D. M. B. A. E. Kallen, Ed., Springer-Verlag, 155–206.

Slutz, R. J., S. J. Lubker, J. D. Hiscox, S. D. Woodruff, R. L. Jenne, D. H. Joseph, P. M. Steurer, and J. D. Elms, 1985: Comprehensive Ocean-atmosphere Data Set, release 1. NOAA Tech. Note, 255 pp. [Available from University of Colorado/National Oceanic and Atmospheric Administration Cooperative Institute for Research in Environmental Sciences, Boulder, CO 80305.]

Ward, M. N., and C. K. Folland, 1991: Prediction of seasonal rainfall in the north Nordeste of Brazil using eigenvectors of sea-surface temperature. *Int. J. Climatol.,* **11,** 711–743.

Yoo, J. M., and J. A. Carton, 1988: Spatial dependence of the relationship between rainfall and outgoing longwave radiation in the tropical Atlantic. *J. Climate,* **1,** 1047–1054.

Zebiak, S. E., 1993: Air–sea interaction in the equatorial Atlantic region. *J. Climate,* **6,** 1567–1586.